J. Micromech. Microeng. **19** (2009) 025027 (12pp) doi:10.1088/0960-1317/19/2/025027

Silicon microcontact printing engines

R R A Syms[1,3], H Zou[2], K Choonee[1] and R A Lawes[1]

[1] Optical and Semiconductor Devices Group, EEE Department, Imperial College London, Exhibition Road, London SW7 2AZ, UK
[2] School of Mechanical Engineering, Dalian University of Technology, Dalian, 116024, People's Republic of China

E-mail: r.syms@ic.ac.uk

Received 13 September 2008, in final form 21 November 2008
Published 26 January 2009
Online at stacks.iop.org/JMM/19/025027

Abstract
A method of self-aligned, microcontact printing that avoids the need for dedicated alignment and stamping equipment is demonstrated. Complete miniature print engines combining elastically supported print heads with alignment structures that mate with corresponding features on etched substrates to allow mechanical registration are constructed from silicon parts. The impression can be transferred manually or using an in-built mechanism such as electrostatic actuation. 10 mm × 10 mm prototypes are fabricated using microelectromechanical systems technology, using a wafer-scale process based on deep reactive ion etching of either bulk silicon or bonded silicon-on-insulator wafers to form all mechanical parts and polydimethylsiloxane spray coating of etched surfaces to form soft stamps. Electromechanical characterization is performed and manual and electrostatic microcontact printing are both demonstrated through 1-hexadecanethiol ink transfer onto gold-coated surfaces over a 5 mm × 5 mm area with a minimum feature size of ≈2 μm.

1. Introduction

Since the demonstration by Kumar and Whitesides of microcontact printing (μCP) in 1993 [1], many new possibilities for sub-micron patterning and structuring have been opened up. Figure 1 shows a schematic of the process. The starting point is a soft stamp, formed by replica moulding from an etched master. In the most widely characterized chemistry, the stamp is soaked in an ethanol solution of alkanethiol ink and dried to remove most of the ethanol. It is then contacted against a gold-coated substrate, where the alkanethiol forms a self-assembled monolayer (SAM) after binding its terminal thiol (–SH) group to the Au [2].

Alkanethiols have the general form $CH_3(CH_2)_nSH$. Extensive surface characterization has shown that alkanethiols chemisorb on Au and rapidly self-organize to form 2–3 nm thick, highly ordered quasi-crystal monolayers, with the alkyl chains $(CH_2)_n$ extending from the (1 1 1) Au surface and tilted at ≈30° [3]. For $n > 11$ this layer is closely packed and significantly defect-free. While SAMs are not sufficiently durable to act as a hard mask during reactive ion etching, they can act as a resist to a selective wet etch, for example allowing the pattern to be transferred through the Au layer using a ferricyanide etch [4].

Resolution is limited by stamp deformation and ink diffusion to ≈100 nm. Stamps are formed from the compliant elastomer polydimethylsiloxane (PDMS) [5]; however, stamp deformation is known to affect dimensional stability [6], and improved pattern transfer is obtained using composite stamps [7]. Stamps can be re-used, and the ability to obtain multiple prints without re-inking is controlled by bulk diffusion of ink in the PDMS to the surface of the stamp [8]. Stamps cannot be completely cleaned of ink, although surface residues can be removed. Consequently, stamp fabrication must be of low cost.

Hexadecanethiol ($n = 15$), octadecanethiol ($n = 17$) and eicosanethiol ($n = 19$) are all suitable alkanethiols for printing on Au. They have been extensively compared, and it has been shown that the 'best' choice (octadecanethiol) is a compromise between the need to limit lateral diffusion of ink during printing and to provide a defect-free SAM for protection during etching. Alkanethiols with lower molecular weight diffuse too rapidly, while those with larger molecular weight self-organize less well [8].

To pattern other substrates, inks must be identified that can form a SAM on the surface concerned and withstand subsequent processing. Alkanethiols have been used to

[3] Author to whom any correspondence should be addressed.

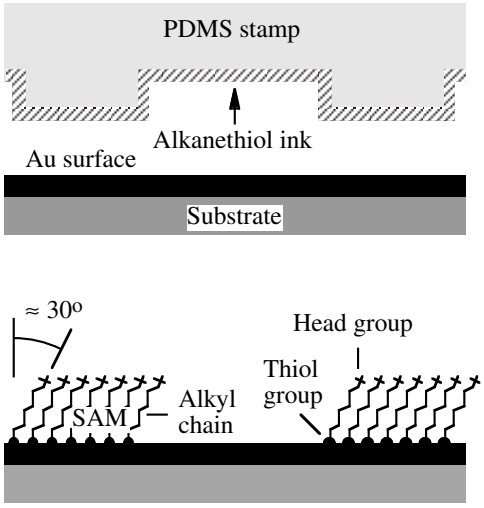

Figure 1. Microcontact printing on Au using a PDMS stamp and alkanethiol (after Whitesides).

pattern many other metals such as Ag [10], Cu [11] and Pd [12], and alkanephosphonic acids have been used for Al [13]. Printed patterns have been transferred from Au to semiconductors such as Si [14] and GaAs [15] by reactive ion etching, and Si has been patterned directly using siloxane SAMs on Si-OH surfaces [16] or alkoxyl SAMs on Si-Cl surfaces [17]. Siloxane SAMs have been used to pattern SiO_2 [18], trichlorosilane SAMs to pattern oxides such as Al_2O_3 and TiO_2 [19] and alkanephosphonic acids to pattern ITO [20]. Reviews of ink/substrate combinations can be found in [21, 22], and there is interest in inks that are less specific to particular substrates [23]. Reviews of selective etchants are also available [24].

Microcontact printing has been adapted to curved surfaces [25], and large-area patterning has been demonstrated with a purpose-built aligner [26]. Applications have been proposed in microelectronics [27] and organic electronics [28]. However, because the surface properties (such as the hydrophobicity) of the SAM can easily be modified, by changing the head group, there is much greater interest in applications in biochemistry and biology than in microfabrication. Particularly, patterning of proteins has been used to localize and control cells [29, 30]. In one approach, μCP is first used to pattern an Au-coated substrate with a hydrophobic SAM. Immersion of the substrate in a different alkanethiol terminated in ethylene glycol groups (e.g. $HS(CH_2)_{11}(OCH_2CH_2)_nOH(EG)_n$, with $n = 2$–7) is then used to surround the patterned areas with a hydrophilic SAM. The hydrophobic areas rapidly and irreversibly adsorb proteins such as fibronectin, laminin vitronectin, heparin and collagen, and hence can provide an extracellular matrix for *in vitro* experiments on cells that are bound to the surface pattern, while the hydrophilic SAM resists protein adsorption [31].

Many applications involve printing on microstructured surfaces [32, 33], and there is particular interest in *in vitro* studies of neurons [34–36], which require alignment to electrodes [37, 38]. At present, alignment is carried out using customized systems that combine three-axis stages with an optical microscope. These differ from conventional mask aligners in avoiding any use of an initial contact to set parallelism and separation. Methods of nanoscale patterning such as nanoimprint lithography [39] and step-and-flash imprint lithography [40] have received considerable investment, and commercial alignment systems have been developed in each case. In contrast, little attention has been paid to equipment for μCP, although arguably it would be too expensive outside the microelectronics industry. There is therefore a case for developing low-cost solutions for aligned μCP.

Microelectromechanical systems (MEMS) technology has the potential to combine much of what is required in silicon. MEMS have evolved considerably over the last 30 years. A key early development was the discovery of anisotropic etching down (1 1 1) planes of crystalline silicon [41]. Since then, new techniques such as deep reactive ion etching (DRIE) of bonded silicon-on-insulator (BSOI) [42] have vastly increased capabilities, allowing robust high-aspect ratio features to be formed in multilayers without restrictions from crystal orientation. A wide range of micro-actuators have also been developed [43]; these typically combine an elastic suspension with an electrostatic, electrothermal, electromagnetic or piezoelectric drive.

In this paper, we use silicon MEMS to integrate features for printing that have already been demonstrated separately (such as a flexure suspension, an actuation mechanism and alignment features) with soft stamps in a complete miniature microcontact printing engine. Some of these concepts have already been applied in a pneumatic 'smart stamp' for nanoimprint lithography [44]. The alignment features mate with corresponding features on substrates to allow self-alignment with a defined separation, and an elastic suspension allows controlled motion of a print head. Actuation may currently be manual or electrostatic. A key issue is the provision of a soft stamp comparable to those formed by PDMS casting, so that the ink transfer process will still operate. Here, soft stamps are formed by spray coating etched silicon surfaces with PDMS after completion of the MEMS fabrication.

Section 2 outlines the concept and presents design rules for an electromechanical system for microcontact printing. Section 3 describes wafer-scale fabrication of prototype print engines in both silicon and bonded silicon-on-insulator materials, with an overall size of 10 mm × 10 mm and a 5 mm × 5 mm printing area. Section 4 presents the results of initial characterization and demonstrates microcontact printing using hexadecanethiol on Au-coated Si with microscale resolution. Both manual and electrostatic printing of single layer patterns are described, and manual multilayer printing is demonstrated. Suggestions for ways to improve print quality and reduce cost and complexity are presented in section 5.

2. Concept and design

In this section, we introduce the concept of a silicon-based microcontact printing engine, and present example design rules for an electrostatically driven system.

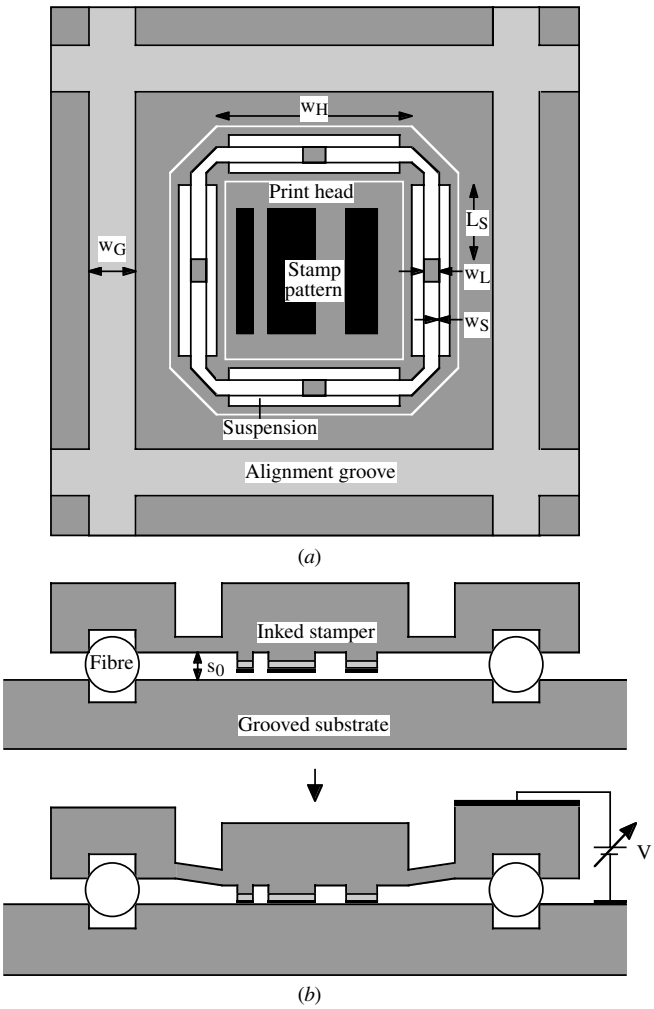

Figure 2. (*a*) Plan and (*b*) section view of a silicon microcontact printing engine.

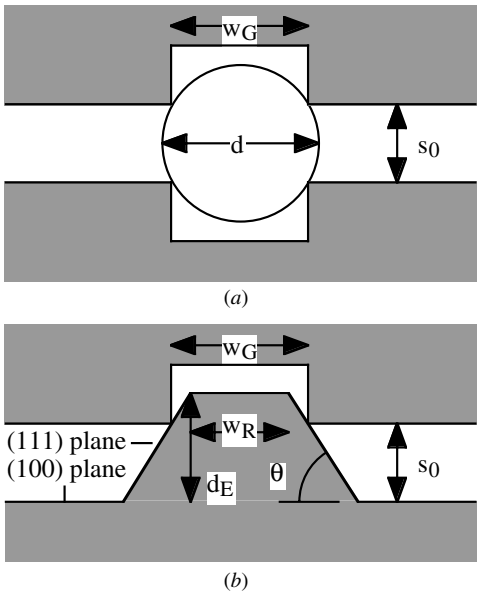

Figure 3. Alignment structures based on (*a*) optical fibres in etched grooves and (*b*) etched rails.

2.1. Concept

Figure 2(*a*) shows a microcontact printing engine, which consists of a small die containing a print head carrying a raised pattern and supported on an elastic suspension allowing out-of-plane deflection. The engine's surround is grooved to mate with a rail pattern arranged on a grid. The device may easily be constructed in single crystal silicon or BSOI. Parts requiring mechanical strength (the print head and surround) are formed in the substrate and flexible parts (the suspension) in a thinner layer. The stamp pattern itself is ideally formed in or coated with PDMS. Figure 2(*b*) shows operation. After coating the stamp with alkanethiol, the engine is placed over a substrate containing compatible alignment features that define its position, parallelism and height s_0. The head is deflected down to print, and finally retracted.

Several possibilities exist for actuation, including manual, pneumatic, piezoelectric or (as shown here) electrostatic methods. Each has advantages and disadvantages. Manual operation is simple and can be used with any substrate, but may result in uncontrolled printing. Piezoelectric actuation can also be used with any substrate but requires specialized materials that over-complicate what must be a low-cost device. Pneumatic actuation is again substrate independent, but requires a membrane suspension and a reliable seal to a plenum chamber above the stamper. In contrast, electrostatic actuation merely requires a conducting device and can be used with any suspension, but requires a conducting substrate and measures to prevent discharge. Because a conducting layer is inherent in alkanethiol-Au microcontact printing, we focus here on manual and electrostatic actuation.

2.2. Self-alignment

Since the process is self-aligning, patterns can be located and overlaid. Many different passive alignment features may be used, including V-grooves and rails formed by anisotropic wet chemical etching, U-grooves formed by DRIE, and optical fibres. Most have been used for optical [45] or electrical [46] connectors. For example, figure 3(*a*) shows U-grooves loaded with sections of optical fibres. This approach allows grooves to be formed in the print engine at the same time as the suspension, and the fibres to provide electrical isolation. In this case, the separation s_0 between stamp and die is determined by in-plane geometry. Using U-grooves of width w_G on each part and spacers of diameter d, we get

$$s_0 = d\{1 - (W_G/d)^2\}^{1/2}. \quad (1)$$

For example, using grooves of width $w_G = 120\ \mu$m and single-mode fibre diameter $d = 125\ \mu$m, we obtain $s_0 = 35\ \mu$m. Smaller separations are, however, hard to achieve due to the limited availability of different fibres and poor tolerance (ds_0/dw_G tends to infinity as s_0 tends to zero). Other alignment structures that have faces with constant slope, such as rails formed by crystal plane etching, may be more appropriate for small separations, but restrict use to Si. Figure 3(*b*) shows a mounting based on a rail of width w_R formed in (1 0 0) Si. In this case, the separation is determined

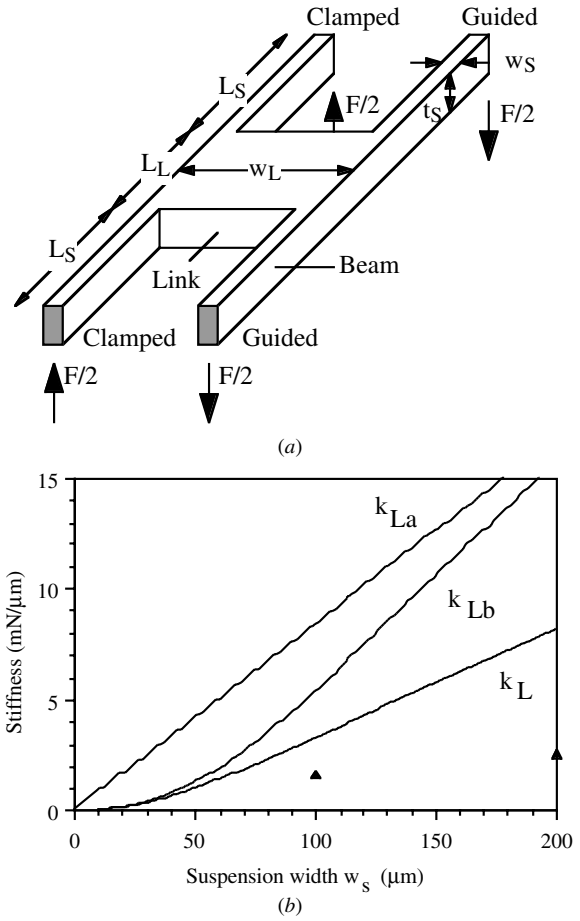

Figure 4. (*a*) Detail of the suspension system; (*b*) theoretical variation of the stiffness terms k_{La}, k_{Lb} and k_L with the suspension width w_S for a suspension thickness $t_S = 80$ μm, suspension length $L_S = 1.6$ mm and link length $w_L = 1$ mm. Discrete points show experimental data.

from the etch depth d_E as

$$s_0 = d_E - 0.5\{w_G - w_R\}\tan(\theta). \quad (2)$$

Here θ is the angle between the (1 0 0) and (1 1 1) planes and $\tan(\theta) = \sqrt{2}$. In this case, small separations may be achieved provided d_E may be suitably controlled.

2.3. Mechanical design

Suitable elastic suspensions include beams, torsion bars and membranes. Here, we consider the example in figure 4(*a*), which consists of four beams of length L_S, width w_S and thickness t_S on each side of a square print head of dimension w_H. Within each set, the bars are arranged in two pairs, connected by a rigid link bar of length w_L. The stiffness of this arrangement is simple to estimate. Deflection will arise from a combination of bending and torsion. Provided the material is linear, and the effects of bending and torsion do not interact, the deflections may be found separately and summed [47]. For example, through bending alone, each bar will deflect as a clamped-guided beam with stiffness [48]

$$k_{L1a} = 12EI_S/L_S^3 \quad (3)$$

Here E is the Young's modulus of the beam material, and I_S is the second moment of area of the cross-section, given by $I_S = w_S t_S^3/12$. Each set of four bars is arranged as a series–parallel combination, so their total stiffness is again k_{L1a}. For all four suspensions together, the combined stiffness is $k_{La} = 4k_{L1a}$.

The contribution of torsion to deflection may be found in a similar way. For a rectangular section measuring $w_S = 2a$ by $t_S = 2b$, the torsion constant is [48]

$$k_T = ab^3\{16/3 - 3.36(b/a)[1 - b^4/12a^4]\} \quad \text{for } a \geqslant b \quad (4)$$

The torque T required to twist one bar through an angle θ is $T = Gk_T\theta/L_S$, where G is the shear modulus of the beam material. If the torque is generated by a force F at a distance w_L, we may write $F = T/w_L$, and if the twist results in a linear displacement Δs of the force we may put $\theta = \Delta s/w_L$. The effective linear stiffness arising from the twist is then $k_{L1b} = F/\Delta s = Gk_T/L_S w_L^2$. In torsion, all bars act in parallel, so the total stiffness is $k_{Lb} = 16k_{L1b}$.

If bending and torsion are considered together, the overall stiffness k_L can be found from $1/k_L = 1/k_{La} + 1/k_{Lb}$. Because of the dependence of k_{Lb} on the link bar length w_L, the relative contribution of bending and torsion to deflection can vary, and if w_L is sufficiently large, torsion dominates. The lines in figure 4(*b*) show the variations of k_{La}, k_{Lb} and k_L with the suspension beam width w_S, assuming a typical elastic layer thickness of $t_s = 80$ μm, a suspension beam length of $L_S = 1.6$ mm and a link bar length of $w_L = 1.0$ mm for comparison with later experimental results. A Young's modulus of $E = 168 \times 10^9$ N m^{-2} and a shear modulus of $G = 61.7 \times 10^9$ N m^{-2} are also assumed, for (1 0 0) Si [49]. For the total stiffness k_L, the curve slowly varies, with a typical stiffness of a few tens of mN per μm. The discrete points are data obtained from experimental devices, as described later.

Although this analysis is approximate, we have verified the basic conclusions by finite element methods, using the commercial software Abaqus 6.8-1. The numerical results showed the estimate of stiffness to be too high by around 50%, largely due to neglect of link bar deformation. They also showed the stiffness to be almost constant (10% variation) for deflections up to 100 μm, suggesting that bending and torsion do not interact significantly.

2.4. Electrostatic operation

To analyse electrostatic operation, we consider the simplified model shown in figure 5(*a*), which in the snap-down phase obeys the well-known analysis of a MEMS varactor [50]. Ignoring the stamp profile, the electrostatic force between the print head and the substrate at voltage V and separation s is $F = 1/2\ \mathrm{d}C/\mathrm{d}s\ V^2$, where $C = \varepsilon_0 A/s$ is the capacitance, $A = w_H^2$ and $\varepsilon_0 = 8.85 \times 10^{-12}$. This force is balanced against the force of the suspension when

$$(\varepsilon_0 A/2s^2)V^2 = K_L(s_0 - s). \quad (5)$$

With some manipulation, equation (5) can be written as the cubic $\eta = (1 - \sigma)\sigma^2$, where $\sigma = s/s_0$ is a normalized separation and $\eta = \varepsilon_0 AV^2/2k_L s_0^3$ is a normalized force. For low η, there are three solutions, of which only the largest is physically realistic. Figure 5(*b*) shows the variation of σ with

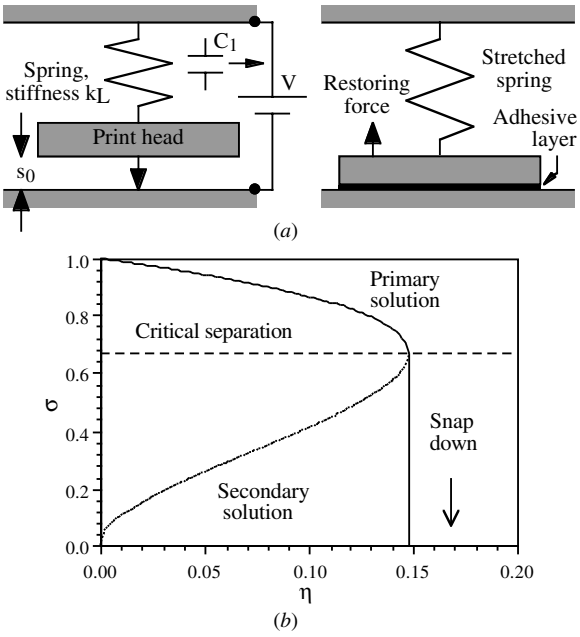

Figure 5. (*a*) Simplified mechanical model of an electrostatically actuated print engine and (*b*) variation of the normalized separation σ with the normalized electrostatic force η.

η, for the two positive roots. When η rises to a critical value η_C, these two roots are repeated, so equation (5) reduces to $(\sigma - \alpha)^2(\sigma - \beta) = 0$. At this point, the elastic force can no longer counter the electrostatic force and snap down occurs. Expanding and equating coefficients, we obtain $\alpha = 2/3$, $\beta = -1/3$ and $\eta_c = \alpha^2\beta = 4/27$. Snap down therefore occurs at a critical separation s_C and a critical voltage V_C given by

$$s_C = 2s_0/3$$
$$V_C = \left(8k_L s_0^3/27\varepsilon_0 A\right)^{1/2}. \tag{6}$$

Voltages are reduced by an increase in the printable area A and increased by a rise in separation s_0 or suspension stiffness k_L, which are needed to detach larger stamps. Figure 6(*a*) shows the variation of V_C with suspension width w_S, for a print head width $w_H = 5$ mm, a suspension beam length $L_S = 1.6$ mm and a link bar length $w_L = 1.0$ mm, a separation $s_0 = 35$ μm and different values of the elastic layer thickness t_S. V_C rises to several hundred volts over the range shown, and larger values of w_S and t_S lead to prohibitive operating voltages.

The high electric fields arising at small separation are likely to cause breakdown in the air gap. One solution may be capacitor stabilization, proposed by Seeger to extend the travel range of parallel plate actuators [51]. A capacitor C_1 is simply placed in series with the actuator, as shown in figure 5(*a*). In this case, it can be shown that snap down does not occur if C_1 is chosen correctly compared with the static capacitance C_0 of the actuator. Furthermore, the voltage dropped across the actuator tends to zero as snap down is approached. However, since the overall operating voltage is increased significantly, further work is required to establish if there is a direct benefit when discharges are likely.

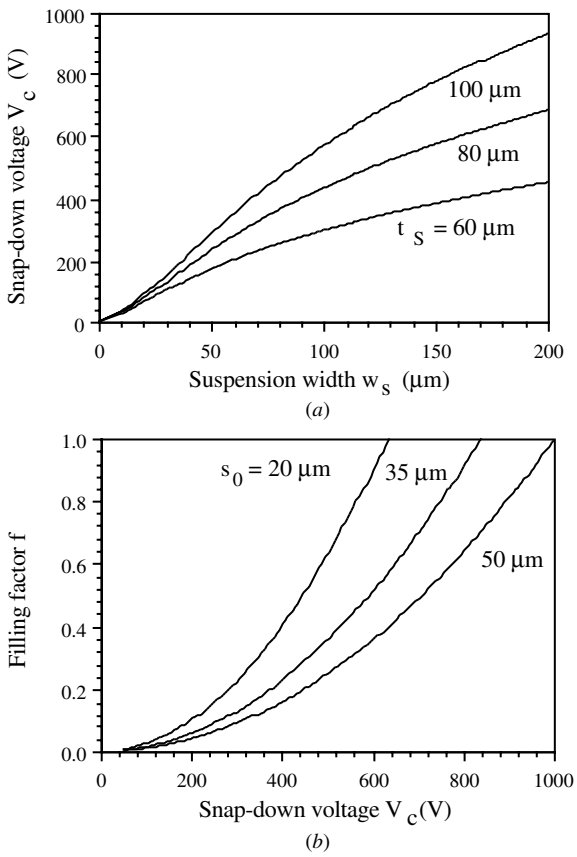

Figure 6. (*a*) Theoretical variation of the snap-down voltage V_C with the suspension width w_S. Parameters are as shown in figure 4, with a print head width $w_H = 5$ mm and a separation $s_0 = 35$ μm. (*b*) Variation of the patternable fraction f of the stamp with V_C, for different s_0.

2.5. Stamp retraction

After the stamp has contacted the die, the voltage may be removed. The print head will retract if the suspension can overcome the adhesion of the alkanethiol. This stick-down problem is common in micromachining [52] and has led to methods for determining the work of adhesion W in microstructures [53]. Assuming that the patterned fraction of the stamp is f, the work required to detach the stamp is fAW. The stamp will detach if the suspension has sufficient stored elastic energy, which requires

$$k_L s_0^2/2 > fAW. \tag{7}$$

Larger spring forces are needed to detach stamps with larger printable areas. Equation (7) may be combined with equation (6) to yield an expression for the maximum filling factor as

$$f = 27\varepsilon_0 V_C^2/16 s_0 W. \tag{8}$$

The work of adhesion of alkanethiols on Au has been studied by atomic force microscopy [54] and is roughly independent of the chain length n, at $W \approx 300\,\mathrm{mJ\,m^{-2}}$ [55]. Figure 6(*b*) shows the variation of f with V_C, assuming the same parameters but different s_0. High filling factors are achievable, but larger factors can be used at lower voltages for small separations.

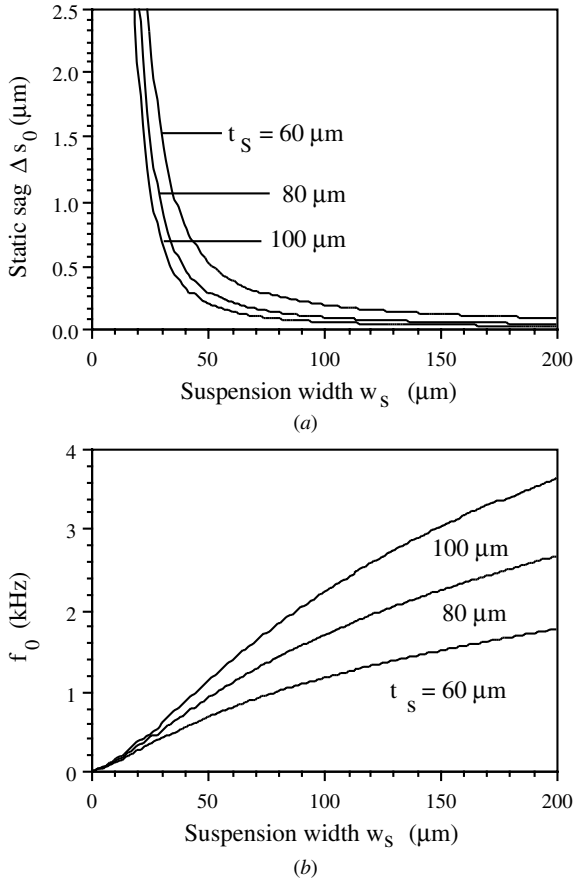

Figure 7. Theoretical variation of (*a*) the static sag Δs_0 and (*b*) the resonant frequency f_0 with the suspension width w_S. Parameters are as shown in figure 6, with a substrate thickness $t_{SUB} = 500\ \mu$m.

2.6. Static sag

The suspension must support the print head without excessive sag due to self-weight. For a block of thickness t_{SUB} and area A formed in a material of density ρ, the static sag Δs_0 is

$$\Delta s_0 = A^2 t_{SUB} \rho g / k_L. \quad (9)$$

Here, $g = 9.81$ m s^{-2}. Figure 7(*a*) shows the variation of Δs_0 with w_S for the parameters above, assuming (again, for comparison with later experiments in Si) that $t_{SUB} = 500\ \mu$m and $\rho = 2330$ kg m^{-3}. For $w_S > 50\ \mu$m, the static sag is sub-micron and may be neglected.

2.7. Dynamic oscillations

After the stamp has been detached, it will oscillate on its suspension. The arrangement shown has linear, rocking and twisting modes. Because of the high mass of the print head, oscillation frequencies are likely to be low. For the primary linear mode, the resonant frequency is

$$f_0 = 1/2\pi (k_L/\rho t_{SUB} A)^{1/2}. \quad (10)$$

Figure 7(*b*) shows the variation of f_0 with w_S for the suspension and print head above. The frequencies rise as the suspension stiffness increases, but are likely to lie in the kHz range. Damping could be controlled using methods developed for accelerometers [56]. Together, these results suggest that an electrostatically driven microcontact print engine may be constructed with the general dimensions given. Design rules may clearly be constructed using similar arguments for other suspension layouts and actuation modes.

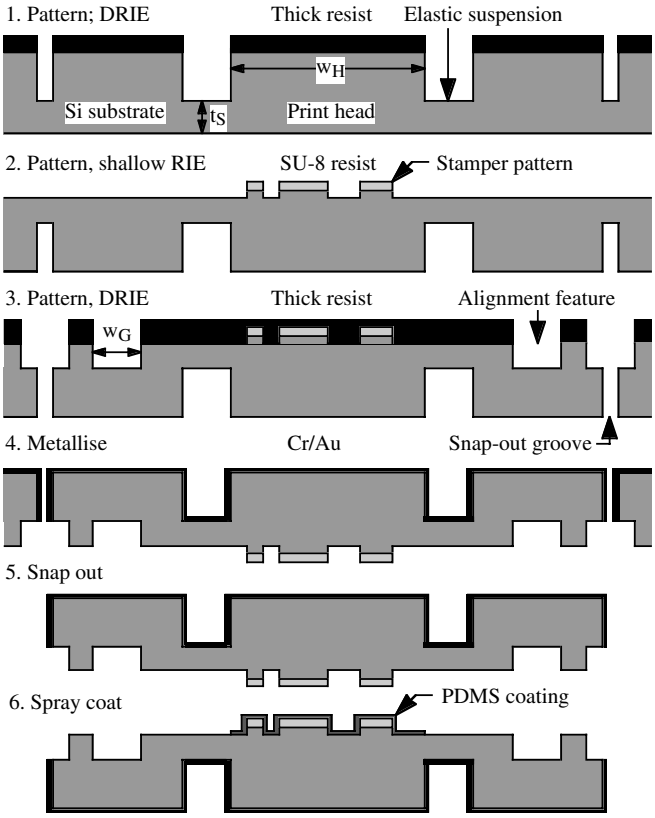

Figure 8. Process flow for device fabrication in single crystal silicon.

3. Fabrication

In this section, we describe processes for wafer-scale fabrication of prototype microcontact printing engines in silicon-based materials.

3.1. Materials and layout

Prototypes have been fabricated in both single-crystal silicon and bonded silicon-on-insulator. Bare silicon is obviously preferable on the grounds of cost. However, BSOI allows accurate definition of the thickness t_S of the elastic layer (here, 80 μm) and hence more controllable operation. In each case, 100 mm diameter (1 0 0) orientated wafers were used. BSOI wafers were obtained from Icemos, Belfast, UK, with a bonded layer thickness of 80 μm and a buried oxide thickness of 2 μm. Prototypes were constructed with the layout of figure 2(*a*), an overall die size of 10 mm × 10 mm and the dimensional parameters of the previous section. Each wafer contained 37 devices.

3.2. Process flow

Figure 8 shows the process flow for bulk silicon. The rear side of the substrate is first patterned with 8 μm thickness

of Shipley AZ9260 resist to define the overall layout, and this pattern is transferred to a set depth (400 μm for t_S = 150 μm) by deep reactive ion etching (step 1). Etching is carried out using a Surface Technology Systems inductively coupled plasma etcher, using a cyclic etching process based on SF_6 and C_4F_8 [57]. The resist is then removed, and the substrate is turned over. The front side is then patterned to define the stamp, using a through-wafer mask-aligner. However, front-to-back alignment is not critical. The stamp pattern is formed by optical exposure of 2 μm thickness of SU-8 2002 epoxy photoresist (Microchem) [58], followed by further 10 μm deep reactive ion etching (step 2). The front side is then patterned again with 8 μm thickness of Shipley AZ9260 resist to define the elastic suspension and alignment grooves. Registration of the two front-side patterns is important since it defines the relative position of the stamp and the alignment grooves. This final pattern is transferred down to meet the original backside etch, using a 5–10 μm thick layer of electroplated Ni (not shown) as an etch stop (step 3).

Similar processing was carried out on BSOI, with the buried oxide defining the mechanical layer thickness. Additional steps were required to remove the etch stop in each case. Remaining resist is then removed, and 300 Å of Cr and 1000 Å of Au are sputtered over the rear of the wafer for electrical contact (step 4). Individual engines are removed for use by breaking small silicon tabs (step 5). To allow the adsorption of alkanethiols, the stamp is spray coated with PDMS through a stencil (step 6), as described in section 4.

3.3. Prototype devices

Figure 9(*a*) shows the rear side of a completed 100 mm wafer. Although fragile, the wafer is robust enough for handling provided the shock is avoided. Figure 9(*b*) shows a detached device mounted on an etched rail system of the type in figure 3(*b*). Figure 10(*a*) shows a SEM view of the front of a detached engine. The print head is at the centre and carries a simple bar pattern consisting of parallel lines of decreasing width down to 2 μm. Figure 10(*b*) shows the rear of the suspension and print head. The latter carries a waffle pattern to reduce mass.

4. Experimental characterization

In this section, we present characterization results for electrostatically operated devices, further details of stamp fabrication and initial demonstrations of microcontact printing.

4.1. Self-alignment

In addition to the use of an etched rail system as shown in figure 9(*b*), self-alignment was demonstrated using substrates carrying grooves formed by DRIE, with standard 125 μm diameter telecoms optical fibre as a spacer. Vertical positions were determined using an optical microscope equipped with a Mitutoyo height gauge. For both types of device, the separation between stamp and substrate was $s_0 \approx 25$ μm. This value is close to but smaller than the design height (35 μm),

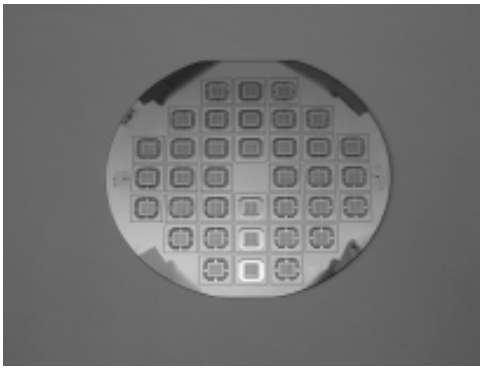

(*a*)

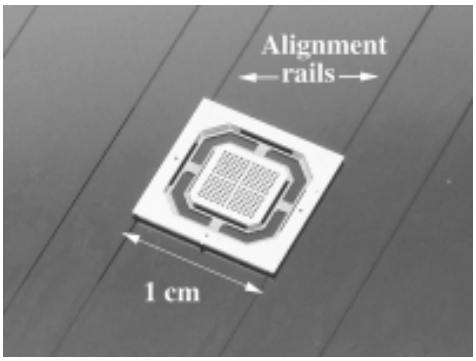

(*b*)

Figure 9. (*a*) Completed wafer; (*b*) contact printing engine mounted on etched alignment rails.

suggesting that the grooves had widened during processing, and confirms the poor tolerance mentioned earlier. There was no discernable static sag.

4.2. Electromechanical characterization

Suspension stiffnesses were determined by measuring the deflection obtained with calibrated weights on the print head, again using a microscope. Figure 11(*a*) shows load–deflection characteristics for BSOI devices with $t_S = 80$ μm and different suspension widths w_S. Each point is the mean of six measurements, and data are shown for two devices for each w_S. The characteristics are linear, and there was no difficulty in obtaining deflections up to 60 μm. The stiffnesses for w_S = 100 μm and 200 μm were obtained from the inverse slope as 1633 μN μm^{-1} and 2615 μN μm^{-1}, respectively. These values are superimposed in figure 4(*b*) and are slightly lower than estimates, presumably due to bending of other parts of the structure. Bare silicon devices had considerably deeper (150 μm) and stiffer suspensions, whose values were hard to measure accurately due to the difficulty of interposing large masses between the device and the microscope objective.

Electrostatic operation was quantified by placing a print engine at a calibrated height above a gold-coated substrate and by applying a voltage between the two. Figure 11(*b*) shows the variation of separation s with voltage, for a BSOI device with 100 μm wide suspension. The initial separation s_0 has been increased to 60 μm using insulated spacers, to improve measurement accuracy. The qualitative agreement with figure 5(*b*) is excellent. However, snap down occurs at

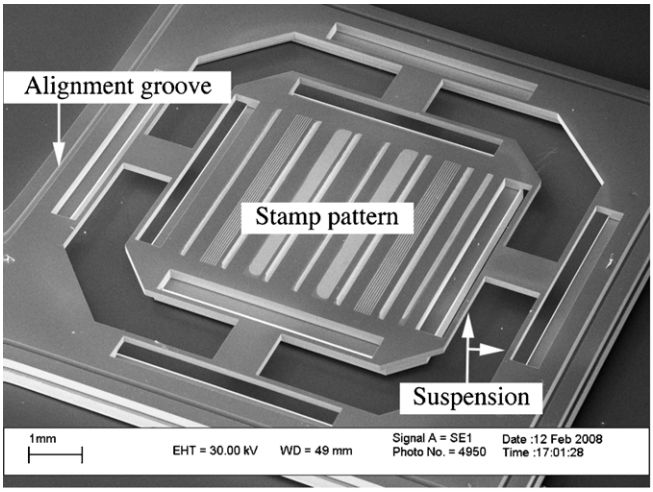

(*a*)

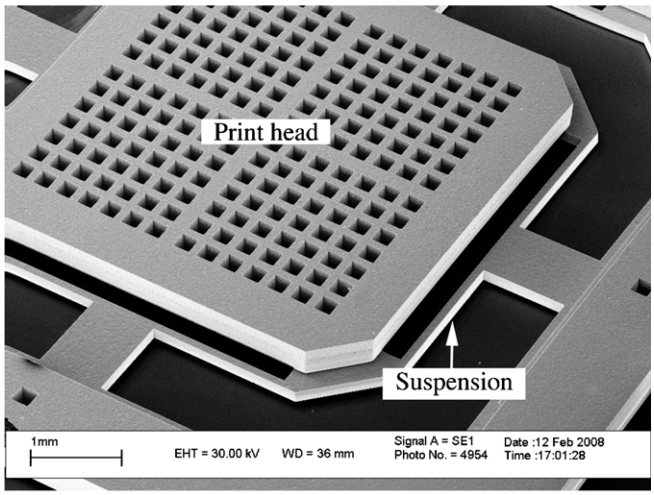

(*b*)

Figure 10. SEM view of (*a*) completed print engine and (*b*) rear side of print head and suspension.

V_C = 370 V, which agrees only approximately with the prediction of equation (5) (V_C = 690 V), suggesting that the print head may have tilted as it deflected.

Figure 11(*b*) also shows the voltage–deflection characteristic for a bare silicon device with similar suspension width. Here the stiffness is so large that $V_C = 800$ V is required to achieve snap down even when s_0 is reduced to 25 μm. Such high voltages are unusable for electrostatically actuated printing, since a dc discharge inevitably occurs during snap down. Although a series resistor was used to limit the current flow, serious damage was then caused to the gold surface. Consequently, low voltages (which imply weak suspensions and small initial separations) were required. This aspect is described in more detail later on.

4.3. Soft stamp fabrication

The conventional route to fabricating a soft stamp, namely to form an embossed PDMS layer at the outset, was incompatible with the subsequent steps used to form the print engine because some raised the temperature above the recommended working range of the material. Under these conditions, the PDMS did

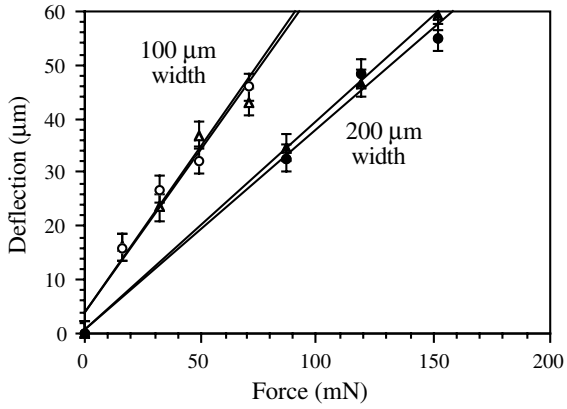

(*a*)

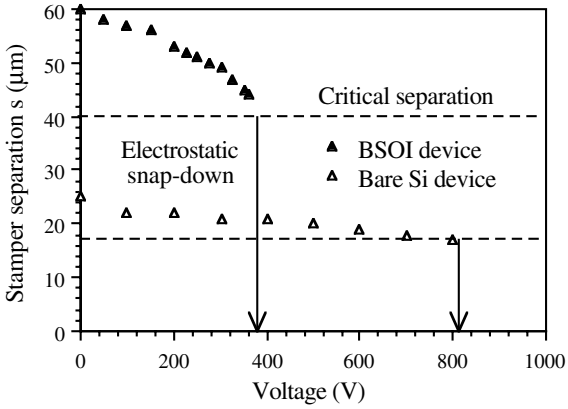

(*b*)

Figure 11. (*a*) Load-deflection characteristics of print engines with different suspension widths w_S; (*b*) voltage-deflection characteristics of engines formed in different substrates.

not appear to adsorb alkanethiols. Embossing at the end of the process was also impractical because of the heavily terraced and fragile nature of the completed wafer. μCP was therefore demonstrated with photopatterned stamps, formed by DRIE of silicon using SU-8 as a hard mask. For example, figure 12(*a*) shows a simple pattern of parallel bars, with 5 μm linewidth. The surface and sidewall qualities are both only moderate, due to poor lithography and slight over-etching.

To allow alkanethiol adsorption, the stamps were spray coated with a thin layer of PDMS, using a stencil to localize the coating. Mixtures of commercially available components from Dow Corning were used to create a PDMS solution with a low enough viscosity for spray coating. Sylgard 184 [59] (which has a very high kinematic viscosity, 412 $\times$ 10^3 cSt) was first mixed with 184 curing agent and 200 Fluid 20 cs [60] (which has a much lower viscosity, 20 cSt) in the proportions 1:0.1:1. The solution was applied in N_2 flow using a modeller's airbrush. With care, a uniform covering $\approx$1 μm thick could be obtained with a small droplet size and without bridging adjacent features, as shown in figure 12(*b*). The PDMS was cured at 100 °C for 15 min and washed in ethanol to extract uncured siloxane.

4.4. Microcontact printing

Microcontact printing was carried out using 1-hexadecanethiol, which was first diluted 0.5 mMol in ethanol.

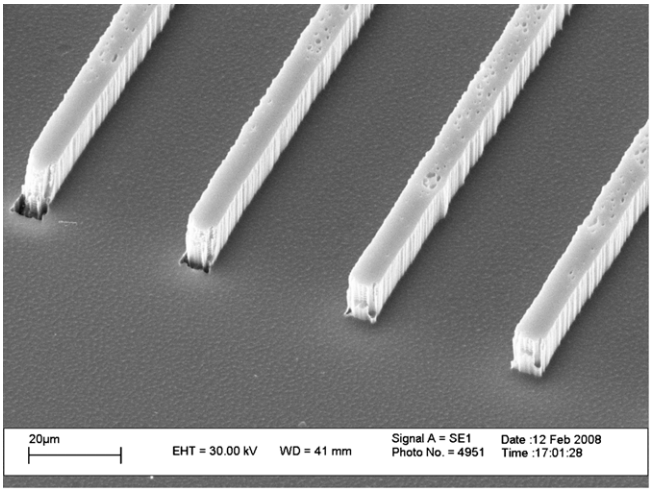

(*a*)

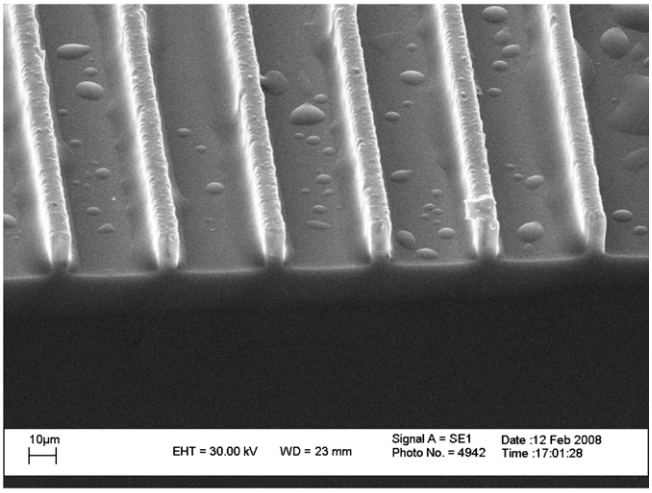

(*b*)

Figure 12. (*a*) Stamp pattern in SU-8 photoresist and Si; (*b*) pattern after spray coating with PDMS.

Stamps were coated with ink using a brush and then blown dry in N_2. Pattern transfer was achieved by contacting the inked stamp to Si surfaces coated with 30 nm Au for around 1 min, and stamps were cleaned of ink residues between prints using ethanol. Patterns were transferred into the gold, by etching exposed Au using a solution of potassium thiosulphate ($K_2S_2O_3$, 0.1 M), potassium hydroxide (KOH, 1 M) and potassium ferricyanide ($K_3Fe(CN)_6$, 0.01 M), an etchant that can achieve a high etch rate (≈5 nm/min) without degrading thiol-derived SAMs [4]. The print quality is not currently uniform over the full area of the stamp. However, it is sufficient to demonstrate concepts.

4.5. Manually actuated printing

Manually actuated printing was performed using bare silicon devices since their suspensions were more robust. Inked print engines were placed on a gold-coated substrate carrying a pair of etched alignment rails, as shown in figures 3(*b*) and 9(*b*), and a pair of tweezers was used to deflect the print head down to the substrate. Single-layer printing was demonstrated first. SEM imaging was used to verify pattern transfer, with back-scattered electron detection to improve image contrast. For example, figure 13(*a*) shows a SEM view of a pattern containing 10 μm wide bars, which have been printed reliably and uniformly.

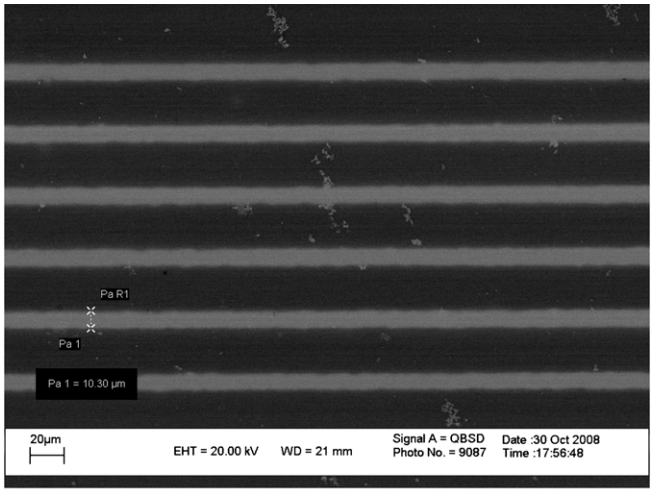

(*a*)

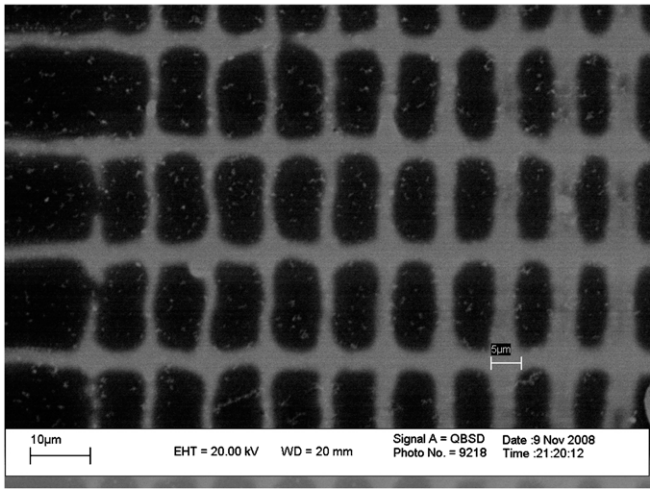

(*b*)

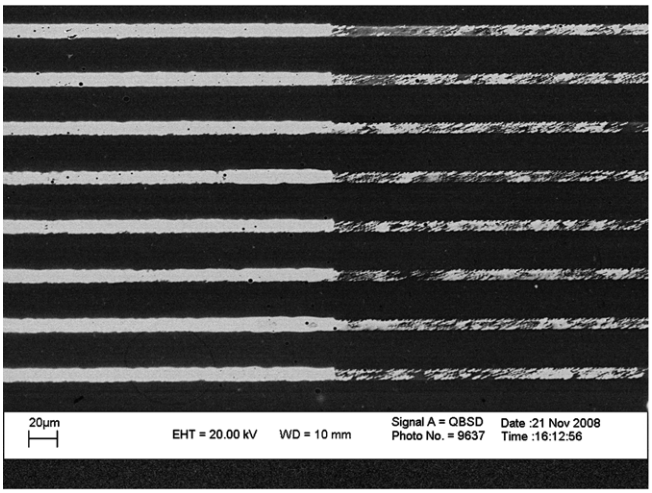

(*c*)

Figure 13. SEM views of transferred pattern in Au, after manually actuated printing and etching, using (*a*) a single imprint, (*b*) a two orthogonal imprints, and (*c*) two shifted imprints.

Multilayer printing was then demonstrated. Figure 13(*b*) shows a pattern formed by printing once, rotating the print engine through 90°, replacing it on the rail and printing a second time. Here, lines of width down to 2 μm have been transferred, although there is some fragmentation of narrow lines attributed to poor stamp quality. The increased pattern width at line intersections is evidence of ink diffusion. To demonstrate aligned printing, which really requires two stamps with complementary patterns, a single stamp was used. A first imprint was made, the stamp was then shifted laterally by ≈1 mm and a second imprint was made. The combined pattern was then transferred into the gold. Figure 13(*c*) shows the result. The boundary between the two imprints is at the centre of the figure. The quality of the second print is unfortunately low, but the overlay error is extremely small.

4.6. Electrostatically actuated printing

Electrostatic actuated printing was more difficult to perform because of the discharge effects described earlier. Discharges appeared to originate from proud features in the pattern, which acted as field concentrators. For example, figure 14(*a*) shows an optical microscope view of a gold surface with a damage pattern roughly matching the stamp (here, rotated by 90° from previous figures). Successful imprints were only obtained with low voltages and limited current flow.

To fix the separation s_0 accurately, a 25 μm thick polyimide sheet was used to support the print engine rather than an insulated alignment feature. BSOI devices with 80 μm thickness and 100 μm wide support beams were used for all successful experiments since these had the weakest suspensions. Devices with shallow (4 μm) etched patterns were also used, to reduce outstanding features. Finally, a 200 MΩ resistor and a 5 nF series capacitor were used to limit current flow at snap down and provide a dc current block. Although the latter effectively corresponded to a stabilizing capacitor, its value was large compared with the static actuator capacitance C_0 (a few pF) that capacitor stabilization was not implemented.

Interesting dynamical effects were observed when the snap-down voltage was still too high. After imposing the voltage, the print head deflected down towards the substrate until a discharge initiated. At this point, the print head retracted until the discharge extinguished, only to repeat the cycle with a period of a few seconds that was presumably determined by the RC time constant of the protection components rather than mechanical time constants.

Reliable printing was only obtained when the separation s_0 was reduced to around 10 μm by placing a small weight on the print head. At this point, the snap-down voltage was ≈200 V. Figure 14(*b*) shows an electrostatically printed pattern. The line definition is worse than that obtained by manual printing. There is no evidence of discharge; however, the quality of the transferred print is degraded by small, dendritic features emanating from each side of the lines. These may be due to ejection of ink droplets during snap down, or to field-driven ink migration. Additional investigation is clearly required to establish the exact cause; however, mitigation

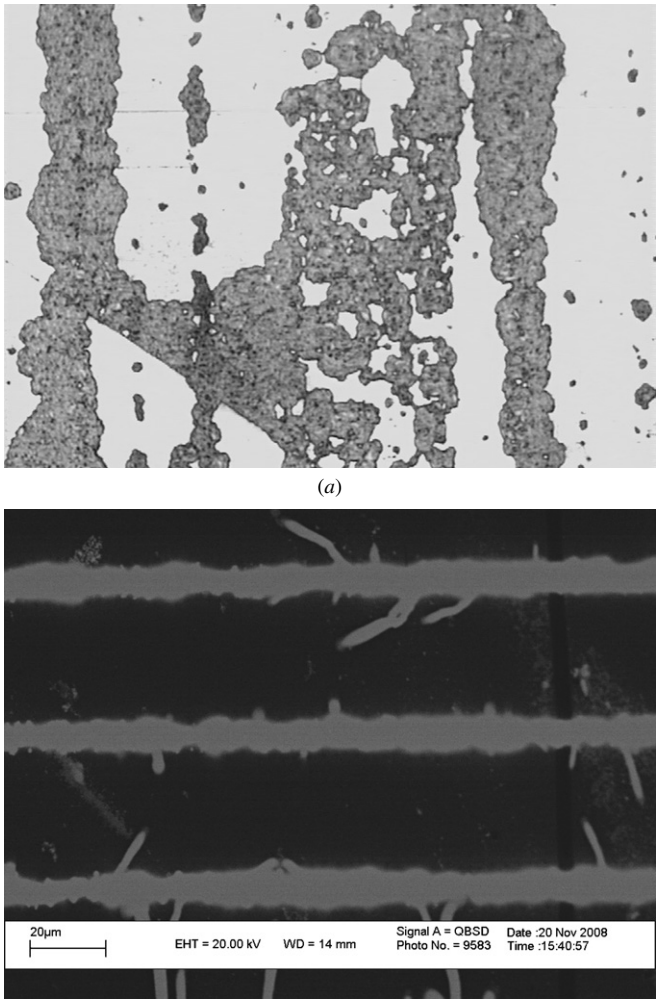

(*a*)

(*b*)

Figure 14. Transferred pattern in Au, formed during electrostatic printing by (*a*) discharge damage at high voltage (optical view) and (*b*) electrostatically actuated contact, ink transfer and etching (SEM view).

is likely to involve a further reduction in operating voltage. Despite this, these initial results demonstrate that soft stamps may be integrated with MEMS structures, single- and double-step printing can be performed, and that electrostatic actuation is possible.

5. Discussion

MEMS technology has been used to construct a silicon microcontact print engine combining a print head, a pattern, a mechanical alignment system, a flexure suspension and an actuator. Simple design rules have been developed for electrostatically driven devices, and it has been shown that printing over an area of tens of mm^2 with a realistic fill factor can be achieved using moderate voltages. Self-alignment and electrostatic operation have been demonstrated using devices formed by DRIE of both bulk silicon and BSOI. Microcontact printing has been demonstrated by transfer of 1-hexadecanethiol onto gold using PDMS-coated stamps with 2 μm minimum feature size. Currently, manual actuation

provides better pattern definition than electrostatic actuation, and problems with discharge at high voltages have been noted. Development is required to reduce feature size, allow properly aligned multilevel printing and extend the printable area. Aspects that require investigation are the alignment accuracy achievable by passive mechanical registration, the maximum die size, the resolution achievable using spray-coated stamps and the merits of electrostatic actuation.

Possible enhancements include integration of features to control discharge and snap down, damp oscillations on release or adjust the stamp position. Potential applications may lie in sensitizing biosensor arrays, where repetitive μCP is required. Similar methods (for example, electrostatic actuation of cantilevers towards the stamp) could be used to transfer some of the complexity to the sensor itself. Other applications may lie in cell biology, where the use of DRIE is likely to be uneconomic and opaque silicon substrates inappropriate. In this case, different materials or alternative fabrication could be used. Wafers could be structured by low-cost crystal plane etching with membrane-suspended print heads. Such wafers would then be robust enough for nanoimprinting of the PDMS stamp. Moulding could also be used to batch fabricate plastic substrates containing alignment features.

Acknowledgments

The authors are grateful to Dr John Stagg for initial work on process development, Dr Munir Ahmad for assistance with PDMS compositions and Dr Tanzi Besant and Dr David Barnes for performing the FEM verification.

References

[1] Kumar A and Whitesides G M 1993 Features of gold having micrometer to centimeter dimensions can be formed through a combination of stamping with an elastomeric stamp and an alkanethiol ink followed by chemical etching *Appl. Phys. Lett.* **63** 2002–4

[2] Bain C D, Troughton E B, Tao Y-T, Evall J, Whitesides G M and Nuzzo R G 1989 Formation of monolayer films by the spontaneous assembly of organic thiols from solution onto gold *J. Am. Chem. Soc.* **111** 321–35

[3] Xia Y N and Whitesides G M 1998 Soft lithography *Angew. Chem.* **37** 551–75

[4] Xia Y, Zhao X-M, Kim E and Whitesides G 1995 A selective etching solution for use with patterned self-assembled monolayers of alkanethiolates on gold *Chem. Matl.* **7** 2332–7

[5] Xia Y N, Tien J, Qin D and Whitesides G M 1996 Non-photolithographic methods for fabrication of elastomeric stamps for use in microcontact printing *Langmuir* **12** 4033–8

[6] Hui C Y, Jagota A, Lin Y Y and Kramer E J 2002 Constraints on microcontact printing imposed by stamp deformation *Langmuir* **18** 1394–407

[7] Odom T W, Love J C, Wolfe D B, Paul K E and Whitesides G M 2002 Improved pattern transfer in soft lithography using composite stamps *Langmuir* **18** 5314–20

[8] Balmer T E, Schmid H, Stutz, Delamarche E, Michel B, Spencer N D and Wolf H 2005 Diffusion of alkanethiols in PDMS and its implications on microcontact printing *Langmuir* **21** 622–32

[9] Bass R B and Lichtenberger A W 2004 Microcontact printing with octadecanethiol *Appl. Surf. Sci.* **226** 335–40

[10] Xia Y N, Kim E and Whitesides G M 1996 Microcontact printing of alkanethiols on silver and its application in microfabrication *Chem. Matl.* **8** 601–3

[11] Xia Y, Kim E, Mrksich M and Whitesides G M 1996 Microcontact printing of alkanethiols on copper and its application in microfabrication *Chem. Mater.* **8** 601–3

[12] Love J C, Wolfe D B, Chabinyc M L, Paul K E and Whitesides G M 2002 Self-assembled monolayers of alkanethiolates on palladium are good etch resists *J. Am. Chem. Soc.* **124** 1576–7

[13] Goetting L B, Deng T and Whitesides G M 1999 Microcontact printing of alkanephosphonic acids on aluminium: pattern transfer by wet chemical etching *Langmuir* **15** 1182–91

[14] Whidden T K, Ferry D K, Kozocki M N, Kim E, Kumar A, Wilbur J and Whitesides G M 1996 Pattern transfer to silicon by microcontact printing and RIE *Nanotechnology* **7** 447–51

[15] Kim E, Whitesides G M, Freiler M B, Levy M, Lin J L and Osgood R M 1996 Fabrication of microstructures on GaAs and GaAs/AlGaAs quantum well material using microcontact printing *Nanotechnology* **7** 266–9

[16] Wang D, Thomas S G, Wang K L, Xia Y and Whitesides G M 1997 Nanometer scale patterning and pattern transfer on amorphous Si, crystalline Si and SiO_2 surfaces using self-assembled monolayers *Appl. Phys. Lett.* **70** 1593–5

[17] Jun Y, Le D and Zhu X-Y 2002 Microcontact printing directly on the silicon surface *Langmuir* **18** 3415–7

[18] Xia Y, Mrksich M, Kim E and Whitesides G M 1995 Microcontact printing of octadecylsiloxane on the surface of silicon dioxide and its application in microfabrication *J. Am. Chem. Soc.* **117** 9576–7

[19] St John P and Craighead H G 1996 Microcontact printing and pattern transfer using trichlorosilanes on oxide substrates *Appl. Phys. Lett.* **68** 1022–4

[20] Breen T L, Fryer P M, Nones R W and Rothwell M E 2002 Patterning indium tin oxide and indium zinc oxide using microcontact printing and wet etching *Langmuir* **18** 194–7

[21] Love C J, Estroff L A, Kriebel J K, Nuzzo R G and Whitesides G M 2005 Self-assembled monolayers of thiolates on metals as a form of nanotechnology *Chem. Rev.* **105** 1103–69

[22] Smith R K, Lewis P A and Weiss P S 2004 Patterning self-assembled monolayers *Prog. Surf. Sci.* **75** 1–68

[23] Burdinski D, Saalmink M, Van Den Berg J P W G and Van Der Marel C 2006 Universal ink for microcontact printing *Angew. Chem., Int. Ed. Engl.* **45** 4355–8

[24] Xia Y N, Zhai X M and Whitesides G M 1996 Pattern transfer: self-assembled monolayers as ultrathin resists *Microelectron. Eng.* **32** 255–68

[25] Jackman R J, Wilbur J and Whitesides G M 1995 Fabrication of submicron features on curved substrates by microcontact printing *Science* **269** 664–6

[26] Burgin T, Choong V E and Maracas G 2000 Large area submicrometer contact printing using a contact aligner *Langmuir* **16** 5371–5

[27] Schmidt G, Tormen M, Müller G, Molenkamp LW, Chen Y, Lebib A and Launois H 1999 Versatile patterning process for semiconductors based on microcontact printing *Electron. Lett.* **35** 1731–3

[28] Rogers J A, Bao Z, Makhija A and Braun P 1999 Printing process suitable for reel-to-reel production of high-performance organic transistors and circuits *Adv. Mater.* **11** 741–5

[29] Chen C S, Mrksich M, Huang S, Whitesides G M and Ingber D E 1998 Micropatterned surfaces for control of

cell shape, position and function *Biotechnol. Prog.* **14** 356–63
[30] Kane R S, Takayama S, Ostuni E, Ingber D E and Whitesides G M 1999 Patterning proteins and cells using soft lithography *Biomaterials* **20** 2363–76
[31] Prime K L and Whitesides G M 1993 Adsorption of proteins onto surfaces containing end-attached oligo(ethylene oxide): a model system for self-assembled monolayers *J. Am. Chem. Soc.* **115** 10714–21
[32] Mrksich M, Chen S C, Xia Y, Dike L E, Ingber D E and Whitesides G M 1996 Controlling cell attachment on contoured surfaces with self-assembled monolayers of alkanethiolates on gold *Proc. Natl Acad. Sci.* **93** 10775–8
[33] Foley J, Schmid H, Stutz R and Delamarche E 2005 Microcontact printing of proteins inside microstructures *Langmuir* **21** 11296–303
[34] St John P M, Kam L, Turner S W, Craighead H C, Isaacson M, Turner J N and Shain W 1997 Preferential glial cell attachment to microcontact printed surfaces *J. Neurosci. Methods* **75** 171–7
[35] Scholl M, Sprössler C, Denyer M, Krause M, Nakajima K, Maelicke A, Knoll W and Offenhäuser A 2000 Ordered networks of rat hippocampal neurons attached to silicon oxide surfaces *J. Neurosci. Methods* **104** 65–75
[36] Oliva A A, James C D, Kingman C E, Craighead H G and Banker G A 2003 Patterning axonal guidance molecules using a novel strategy for microcontact printing *Neurochem. Res.* **28** 1639–48
[37] James C D *et al* 2000 Aligned microcontact printing of micrometer-scale poly-l-lysine structures for controlled growth of cultured neurons on planar microelectrode arrays *IEEE Trans. Biomed. Eng.* **47** 17–21
[38] Lauer L, Ingebrandt S, Scholl M and Offenhäusser A 2001 Aligned microcontact printing of biomolecules on microelectronic device surfaces *IEEE Trans. Biomed. Eng.* **48** 838–42
[39] Chou S Y, Krauss P R and Renstrom P J 1996 Nanoimprint lithography *J. Vac. Sci. Tech.* B **14** 4129–33
[40] Sreenivasan S V, Willson C G, Schumaker N E and Resnick D J 2001 Low-cost nanostructure patterning using step and flash imprint lithography *Proc. SPIE* **4608** 187–94
[41] Bean K E 1978 Anisotropic etching of silicon *IEEE Trans. Electron Devices* **25** 1185–93
[42] Klaassen E H, Petersen K, Noworolski J M, Logan J, Maluf N I, Brown J, Storment C, McCulley W and Kovacs T A 1996 Silicon fusion bonding and deep reactive ion etching: a new technology for microstructures *Sensors Actuators* A **52** 132–9
[43] Fujita H 1998 Microactuators and micromachines *Proc. IEEE* **86** 1721–32
[44] Pedersen R H, Hansen O and Kristensen A 2008 A compact system for large area thermal nanoimprint lithography using smart stamps *J. Micromech. Microeng.* **18** 055018
[45] Schroeder C M 1977 Accurate silicon spacer chips for an optical fiber cable connector *Bell Syst. Tech. J.* **57** 91–7
[46] Larsson M P and Syms R R A 2004 Self-aligning MEMS in-line separable connector *IEEE/ASME J. Microelectromech. Syst.* **13** 365–76
[47] Gere J M and Timoshenko S P 1999 *Mechanics of Materials* 4th edn (Cheltenham: Stanley Thornes) section 8.5
[48] Young W C 1989 *Roark's Formulas for Stress and Strain* 6th edn (New York: McGraw-Hill)
[49] Greenwood J C 1988 Silicon in mechanical sensors *J. Phys. E: Sci. Instrum.* **21** 1114–28
[50] Osterberg P M and Senturia S D 1997 M-TEST: a test chip for MEMS material property measurement using electrostatically actuated test structures *J. Microelectromech. Syst.* **6** 107–18
[51] Seeger J L and Crary S B 1997 Stabilization of electrostatically actuated mechanical devices *Proc. Transducers '97 (Chicago, IL, 16–19 June 1997)* pp 1133–6
[52] Tas N, Sonnenberg T, Jansen H, Legtenberg R and Elwenspoek M 1996 Stiction in surface micromachining *J. Micromech. Microeng.* **6** 385–97
[53] Mastrangelo C H and Hsu C H 1992 A simple experimental technique for the measurement of the work of adhesion of microstructures *Proc. Solid-State Sensor and Actuator Workshop (Hilton Head Is., SC, 25 June)* pp 208–12
[54] Beach E R, Tormoen G W and Drelich J 2002 Pull-off forces measured between hexadecanethiol self-assembled monolayers in air using an atomic force microscope: analysis of surface free energy *J. Adhesion Sci. Tech.* **16** 845–68
[55] Subramanian S and Sampath S 2005 Effect of chain length on the adhesion behaviour of *n*-alkanethiol self-assembled monolayers on Au (1 1 1): an atomic force microscope study *J. Phys.* **65** 753–61
[56] Tschan T, de Rooij N and Bezinge A 1992 Damping of piezoresistive silicon accelerometers *Sensors Actuators* A **32** 375–9
[57] Hynes A M, Ashraf H, Bhardwaj J K, Hopkins J, Johnston I and Shepherd J N 1999 Recent advances in silicon etching for MEMS using the ASE^{TM} process *Sensors Actuators* **74** 13–7
[58] Microchem Corporation SU-8 200 Product description: Permanent epoxy negative photoresist http://www.microchem.com
[59] Dow Corning Corporation Product information: Sylgard 184 Silicone elastomer Form 10-898F-01 http://www.dowcorning.com
[60] Dow Corning Corporation Product information: low viscosity silicone fluids, 200 Fluid 20 cs Form 25-941-97 http://www.dowcorning.com